Title

Epitaxial stabilization of thin films of the frustrated Ge-based spinels

Journal

Physical Review Materials, 5(6)

ISSN

2476-0455

Authors

Vasiukov, Denis M

Kareev, Mikhail

Wen, Fangdi

et al.

Publication Date

2021-06-01

DOI

10.1103/physrevmaterials.5.064419

Peer reviewed

Epitaxial stabilization of thin films of the frustrated Ge-based spinels

Denis M. Vasiukov,[1,2,*] Mikhail Kareev,[1] Fangdi Wen,[1] Liang Wu,[1] Padraic Shafer,[3] Elke Arenholz,[3,4] Xiaoran Liu,[1,5] and Jak Chakhalian[1]

[1]*Department of Physics and Astronomy, Rutgers University, Piscataway, New Jersey 08854, USA*
[2]*Division of Synchrotron Radiation Research, Department of Physics, Lund University, P.O. Box 118, Lund 221 00, Sweden*
[3]*Advanced Light Source, Lawrence Berkeley National Laboratory, Berkeley, California 94720, USA*
[4]*Cornell High Energy Synchrotron Source, Cornell University, Ithaca, New York 14853, USA*
[5]*Beijing National Laboratory for Condensed Matter Physics and Institute of Physics, Chinese Academy of Science, Beijing 10019, People's Republic of China*

Frustrated magnets can host numerous exotic many-body quantum and topological phenomena. $GeNi_2O_4$ is a three-dimensional $S = 1$ frustrated magnet with an unusual two-stage transition to the two-dimensional antiferromagnetic ground state, while $GeCu_2O_4$ is a high-pressure phase with a strongly tetragonally elongated spinel structure and magnetic lattice formed by $S = 1/2$ CuO_2 linear chains with frustrated interchain exchange interactions and exotic magnetic behavior. Here, we report on the thin-film epitaxial stabilization of these two compounds. The developed growth mode, surface morphology, crystal structure, and copper valence state were characterized by *in situ* reflection high-energy electron diffraction, atomic force microscopy, x-ray reflectivity, x-ray diffraction, x-ray photoelectron spectroscopy, and resonant x-ray absorption spectroscopy. Our results pave an alternative route to the comprehensive investigation of the puzzling magnetic properties of these compounds and the exploration of emergent features driven by strain.

Introduction. Research on magnetic systems possessing frustration, low dimensionality, or their combination, is a very active and fruitful subfield with a great potential for emergent phenomena, new states of matter, and exotic excitations exemplified by spin ice, quantum spin liquids, and spin-charge separation to name a few [1–4]. Despite a plethora of interesting theoretical proposals the mapping of theory to realistic material systems still remains a formidable challenge, particularly due to the demand for high-quality materials that can host such exotic phenomena and states [3,5]. As one of the alternatives to the solid-state chemistry routes, ultrathin films may be a viable option to address the challenge.

Among the magnetically frustrated materials, complex oxides with the spinel structure are of special interest. Spinel oxides have the general formula AB_2O_4, composed of a cubic close-packed sublattice of anions in which $1/8$ of the tetrahedral (A-site) and $1/2$ of the octahedral (B-site) interstices are filled by cations. In the absence of distortions, the spinel crystallizes in the cubic space group $Fd\bar{3}m$ and the B-site cations form a network of corner-shared tetrahedra (also termed as "pyrochlore" sublattice) that can potentially trigger the strongest frustration in three dimensions [6]. Following this direction, the so-called "4-2" spinel family with germanium on the A site is particularly interesting (general formula $Ge^{4+}B_2{}^{2+}O_4$), as this class of compounds has a magnetically inactive A site; hence, their magnetic properties are solely determined by the pyrochlore sublattice.

In this paper, we report on epitaxially stabilized thin films of two members of the "4-2" spinel family, $GeNi_2O_4$ (GNO) and $GeCu_2O_4$ (GCO), which exhibit very different low-dimensional magnetic behavior. The bulk GNO undergoes a peculiar two-stage phase transition into a two-dimensional (2D) magnetic ground state [7–12], while the bulk GCO shows a multiferroic transition with interacting 1D $S = 1/2$ chains [13–16].

In GNO the B-site Ni^{2+} has the $3d^8$ electronic configuration, which adopts a nondegenerate electronic term ${}^3A_{2g}$ with negligible single-ion anisotropy. The nondegeneracy of Ni^{2+} indicates that frustration cannot be relieved via structural distortion driven by the cooperative Jahn-Teller effect, making this pyrochlore lattice of isotropic $S = 1$ spins, shown in Fig. 1(a), a promising candidate for unusual magnetic phenomena. Indeed, a study of $NaCaNi_2F_7$ revealed a continuum of quantum fluctuations characteristic for a Coulomb phase with only a spin-glass-like freezing transition [18]. In contrast to this case, the unusual sequence of magnetic transitions is observed in bulk GNO at low temperatures, leading to an antiferromagnetically ordered ground state with a propagation vector $q = (\frac{1}{2}\ \frac{1}{2}\ \frac{1}{2})$ corresponding to the rhombohedral lattice system [19]. Upon this transition the B site splits magnetically into alternating kagome and triangular planes along the (111) direction, which form a set of intrinsically 2D frustrated sublattices.

More detailed recent studies show that this antiferromagnetic state is developed through two consecutive first-order phase transitions separated by ~0.7 K ($T_{N1} = 12.1$ K and $T_{N2} = 11.4$ K) without any measurable structural distortion [7–9,20]. A subsequent muon-spin relaxation experiment suggested that these two transitions correspond to a distinct ordering of two magnetic subsystems [10]. Based on the single-crystal neutron elastic scattering data [11] it was

*vasyukov@physics.msu.ru

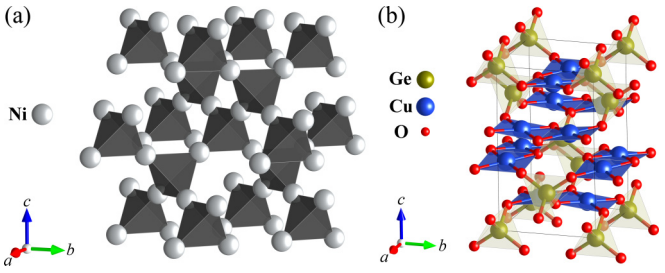

FIG. 1. Crystal structures of $GeNi_2O_4$ and $GeCu_2O_4$ spinels. (a) In GNO the *B*-site sublattice of Ni^{2+} ions forms an ideal pyrochlore sublattice of corner-shared tetrahedra (the Ge and O ions are omitted for clarity). (b) The large tetragonal elongation in GCO results in the effective square-planar coordination of Cu^{2+} ions, therefore the *B*-site sublattice can be regarded as a set of alternating mutually perpendicular layers of 1D chains. These structure figures were prepared using VESTA 3 software [17].

concluded that the first transition (T_{N1}) corresponds to a magnetic ordering only within the kagome planes (each plane has ferromagnetic ordering stacked antiferromagnetically) while the triangular planes become magnetically ordered at the second transition (T_{N2}). Strikingly, the saturated magnetic moment of the triangular planes remains two times smaller than one of the kagome planes [9,11,21], although in the absence of distortions all Ni^{2+} ions are crystallographically equivalent. A strong magnetic anisotropy of the ground state was demonstrated in the single-crystal experiments with an applied magnetic field [21,22]. This highly unusual magnetic behavior seems to be closely related to the $Gd_2Ti_2O_7$ with a pyrochlore structure which shows similar magnetic transitions [23].

The specific-heat data indicate several puzzling features, which remain unexplained. These include the presence of substantial magnetic correlations in the paramagnetic state despite the low frustration factor ($f = \Theta_{CW}/T_N \sim 0.7$), the coexistence of gapped and gapless spin waves, and the missing of ~40 % of the expected magnetic entropy [12]. Furthermore, unexpectedly the change in magnetic entropy is almost equal for both phase transitions [8,12], which clearly contradicts the picture of two separate orderings in the kagome and triangular planes (as a triangular lattice contains three times less Ni^{2+} ions relative to the kagome lattice).

As for the second synthesized spinel, GCO is a recoverable high-pressure phase with the hausmannite structure type (space group $I4_1/amd$). Interestingly, it is only the second tertiary oxide discovered within the ternary Ge-Cu-O system [24] while the first one is the celebrated $GeCuO_3$ with 1D antiferromagnetic $S = 1/2$ chains, and the first discovered spin-Peirls transition (i.e., spin pairing with a valence bond formation) among the inorganic compounds [25]. GCO has a tetragonally distorted spinel structure in which the octahedral *B* site is occupied by the Cu^{2+} Jahn-Teller active ions. Due to the large Jahn-Teller distortion, the local coordination of Cu^{2+} ions can be described as almost square planar with an in-plane Cu-O distance of 1.939 Å and the apical oxygens located at 2.504 Å [24]. As shown in Fig. 1(b), such a large distortion allows to consider this spinel structure as comprised of alternating mutually perpendicular layers of 1D CuO_2 $S = 1/2$ chains interconnected via GeO_4 tetrahedra. The 1D nature of magnetic interactions within the $S = 1/2$ chains is supported by the magnetic susceptibility data that show the characteristic Bonner-Fisher behavior with the ratio of interchain to intrachain exchange couplings $J'/J \sim 0.16$ [13]. The susceptibility data also indicate the onset of long-range magnetic ordering at 33 K [13].

Despite such a large tetragonal distortion of the pyrochlore sublattice, the magnetic interaction between Cu ions in $GeCu_2O_4$ remains frustrated, in close analogy to the Cs_2CuCl_4 case, where the frustrated interchain coupling results in the exotic "triplon" bound state that readily moves between chains [26]. Theoretically, such an anisotropic pyrochlore lattice was mapped onto a 2D crossed-chain model [27], which predicts the formation of a valence-bond solid with a crossed-dimer state in the limit of small J'/J [27]. However, contrary to the model calculations, a density-functional theory (DFT) study of GCO suggests the formation of a spiral magnetic ground state [28]. A subsequent neutron powder diffraction experiment revealed the presence of collinear antiferromagnetism at low temperatures with an unexpected up-up-down-down (i.e., $\uparrow\uparrow\downarrow\downarrow$) spin ordering pattern along the chains [14]. This unusual ordering pattern was attributed to the presence of a biquadratic exchange interaction active in this compound [14] while an *a posteriori* DFT study argued that the actual reason is the negligibly small nearest-neighbor coupling [29]. Surprisingly, two independent groups recently reported spin-induced multiferroicity in GCO emerging at $T_N \sim 33$ K [15,16], which is incompatible with any theoretically proposed or experimentally determined magnetic structures [14,27,28]. To date, the nature of multiferroicity in GCO remains largely unknown.

Taking into account the puzzling magnetism of these compounds and the fact that epitaxial strain can alter the underlying microscopic Hamiltonian of a system, fabricating thin films of GNO and GCO is of great interest since it can potentially shed light on the open questions about the magnetic behavior of the bulk crystals and may lead to new emergent quantum states. Moreover, in the bulk form GCO is only stable at high pressure (~4 GPa [24]) and its high-pressure solid-state synthesis is difficult and yields only *micron-sized* single crystals hindering the application of many important probes. The epitaxial strain can help to stabilize phases which are otherwise unstable at ambient pressure in the bulk [30], therefore exploring the fabrication of GCO thin films can offer alternative opportunities for realizing large-area single crystals.

Here, we report on a successful fabrication of GNO and GCO thin films by means of pulsed laser deposition. The developed growth mode, surface morphology, film thickness, and crystal structure were characterized by *in situ* reflection high-energy electron diffraction (RHEED), atomic force microscopy (AFM), x-ray reflectivity (XRR), and x-ray diffraction (XRD). Stoichiometry of the films and ion valency were investigated by x-ray photoelectron spectroscopy (XPS). Electronic states in the GNO film were further studied by synchrotron-based resonant x-ray absorption spectroscopy (XAS) on the Ni *L* edge and O *K* edge. The combination of advanced tools confirms the successful epitaxial growth of high-quality (001)-oriented GCO and GNO thin films.

Stabilization of the $GeNi_2O_4$ *thin film.* We begin with a description of the details of GNO growth. Taking into account

that the bulk magnetic ground state in GNO has $q = (\frac{1}{2}\ \frac{1}{2}\ \frac{1}{2})$, it is of particular interest to obtain an epitaxially strained film grown in the direction which is noncollinear to this propagation vector. For this reason we have chosen a (001)-oriented $MgAl_2O_4$ (MAO) substrate with a spinel structure for the deposition.

The UV laser (KrF excimer laser with 248 nm wavelength) was operated at a 3 Hz repetition rate with 2.7 J/cm^2 energy density per pulse to ablate a stoichiometric $GeNi_2O_4$ target. All films were deposited on a substrate of 5×5 mm^2 area with an average surface roughness of $S_a \sim 100$ pm heated to 700 °C as measured by a pyrometer under 6 mTorr of pure oxygen. After deposition, samples were annealed at the growth condition and then cooled down to room temperature with an initial rate of 15 °C/min under the same oxygen pressure. All experimental data presented below were collected using the same film.

The deposition process was monitored *in situ* by high-pressure RHEED. The representative RHEED patterns with an indexed zero-order Laue zone of the substrate and fabricated film are presented in Fig. 2(a). As expected for two isostructural compounds the patterns are similar, including identical higher-order Laue zones. The intensity of the specular reflection shows only an initial reduction at the start of the deposition, followed by a rapid recovery that remains constant without any evident oscillations during further deposition. The well-developed streak pattern shown in Fig. 2(a) indicates that the GNO film grows in the step-flow mode [32].

X-ray reflectivity and diffraction measurements were performed with an Empyrean diffractometer using Cu $K\alpha$ radiation. A fit of the XRR data [Fig. 2(b)] yields a surface roughness $S_a = 240(20)$ pm, which is in a good agreement with the AFM results (∼200 pm); both XRR and AFM data confirm the development of a smooth surface morphology of the GNO film. In addition, fitting results of the XRR data yield a film thickness of 11.79(4) nm. The 2Θ-ω scan shown in Fig. 2(c) contains reflections of both the substrate (red) and two reflections of the GNO film (blue). These peaks are indexed as (004) and (008) reflections, confirming the (001) orientation of the film with no other secondary chemical phases present. As the bulk lattice parameter of GNO is $a = 8.22$ Å [33], growth on the MAO substrate ($a = 8.08$ Å) should result in a 1.7% in-plane compressive strain, elongating the out-of-plane lattice constant. Indeed, from our diffraction data we have determined that the out-of-plane lattice constant is 8.376(5) Å, which is consistent with compressive strain.

The XPS spectra were measured by a Thermo Scientific K-Alpha XPS spectrometer with monochromated Al $K\alpha$ radiation. Stoichiometry of the GNO film was determined in high-resolution core-shell scans around the $2p$ state of Ge and Ni and the $1s$ state of O. The analysis of XPS data results in Ge : Ni : O = 1 : 1.98 : 4.24 which is consistent within the experimental uncertainty with the desired $GeNi_2O_4$ composition (the deviation in the oxygen value from the ideal stoichiometric ratio is due to the surface exposed to the ambient). Figure 3(a) shows a characteristic core-shell Ni $2p$

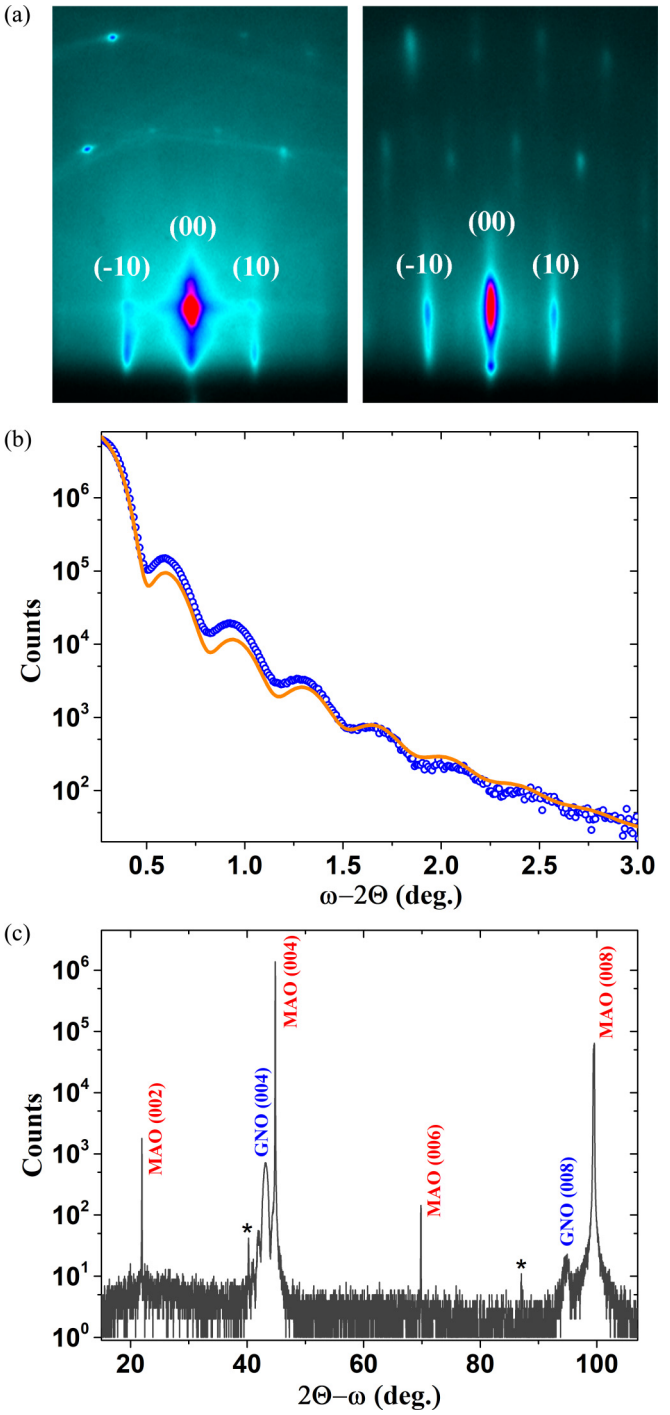

FIG. 2. Characterization of the grown GNO thin film. (a) On the left, the RHEED pattern of the (001)-oriented MAO substrate at 650 °C, and on the right, the RHEED pattern of the grown GNO film at room temperature. (b) The fit of the XRR curve for the same sample yields 11.79(4) nm film thickness and 240(20) pm surface roughness. (c) 2Θ-ω x-ray diffraction scan along the 00l direction. The scan contains allowed reflections of the substrate and fabricated film together with two forbidden reflections (002 and 006) of the substrate which arise because of the Umweganregung effect [31]. Asterisks mark (004) and (008) peaks of the substrate due to residual K_β radiation.

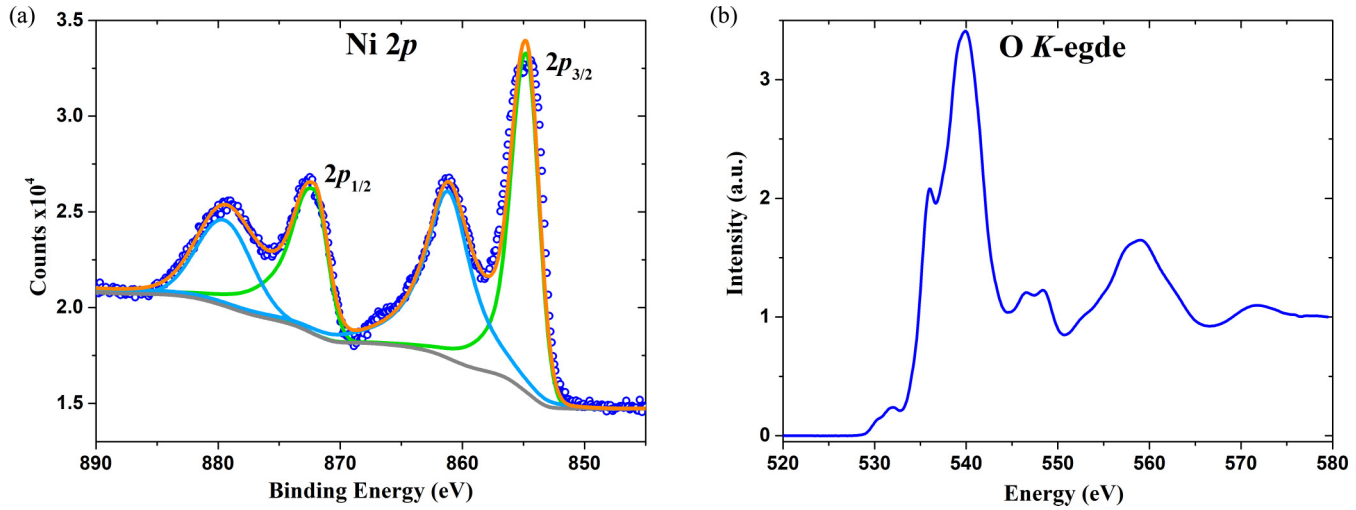

FIG. 3. XPS and oxygen K-edge XAS spectra of the GNO thin film. (a) High-resolution XPS scan of Ni $2p$ states shows the spin-orbit split doublet (green) together with satellite features (light blue). The background line is shown in gray color. Unsplitted doublet confirms that the film contains Ni only in a single valence state. (b) Oxygen K-edge XAS spectrum demonstrates the absence of the sharp prepeak feature that signifies the d^8 electron configuration of Ni^{2+} ions without a significant admixture of configurations with oxygen p holes (e.g., d^9L).

scan. As seen, the energy position of the Ni $2p_{3/2}$ peak at 856.5 eV and the absence of any peak splitting imply the expected single valency of Ni in the film.

To further investigate the electronic state of Ni and O away from the surface, we carried out XAS experiments at beamline 4.0.2 of the Advanced Light Source (Lawrence Berkeley National Laboratory). The oxygen K-edge scan shown in Fig. 3(b) is very similar to the theoretical line shape [34] and does not show any sizable pre-edge intensity around 529 eV, reflecting only a small contribution of configurations with ligand holes (e.g., $3d^9L$) to the electronic state of the Ni ion. Furthermore, in accord with the XPS data the Ni L-edge line shape corresponds to Ni in the 2+ state. The simulated spectrum of Ni^{2+} shown in Fig. 4 corroborates the divalent nature of the Ni ions [35]. An optimization of the calculated line shape to the experimental data yields the following atomic parameters: crystal-field splitting $10Dq = 0.9$ eV, charge-transfer gap of 4 eV, and hopping integrals $V_{e_g} = 2.5$ eV and $V_{t_{2g}} = 1.0$ eV; those values are in agreement with the values of Ni^{2+} reported for NiO [36].

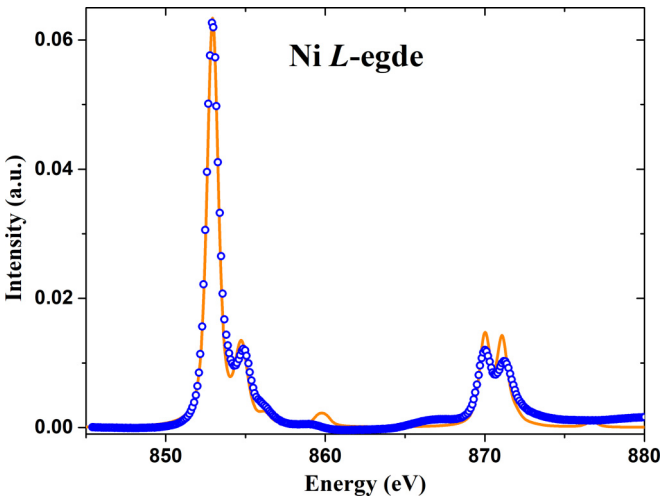

FIG. 4. Ni L-edge XAS spectrum of the GNO film. Blue dots are the measured data whereas the orange line shows the simulated spectrum of Ni^{2+}.

Stabilization of the $GeCu_2O_4$ *thin film.* In the case of GCO, the choice of a suitable substrate is not obvious. Since the bulk $GeCu_2O_4$ is stable only above 4 GPa [24], it is natural to select a substrate offering compressive strain. However, due to the very large tetragonal elongation along the c axis, the GCO lattice is strongly compressed in the ab plane, leading to no commercially available crystals with the same spinel structure to provide a suitable compressive strain in the ab plane [37]. As a compromise, we selected two substrates for our experiments: (i) (001)-oriented $SrTiO_3$ (STO) with a cubic perovskite structure, which would result in compressive strain, and (ii) a (001)-oriented MAO spinel substrate, which is isostructural to GCO but provides moderate *tensile* strain.

For the extensive series of depositions on (001)-oriented STO we varied both substrate temperatures from 470 to 700 °C and background oxygen pressure from 5 to 100 mTorr. The GCO phase failed to stabilize under any of these growth conditions, and only a Cu_2O phase with Cu ions in the +1 oxidation state readily forms at substrate temperatures above 600 °C and low oxygen pressures.

Next, we repeated a series of depositions on the (001)-oriented MAO substrate. At a low oxygen pressure of ∼5 mTorr and in the temperature range 600–700 °C, all the samples stabilize into the Cu_2O phase, akin to the growth on the STO substrate at these conditions. However, upon increasing the oxygen pressure above 50 mTorr, the $GeCu_2O_4$ phase appears to be stabilized within the temperature range of 600–700 °C. Further optimization of the growth condition confirmed that the best-quality GCO films can be obtained at 50 mTorr of O_2 and 600 °C substrate temperature. After deposition all samples were annealed at the growth condition and then gradually cooled down (15 °C/min) to room temperature

at the same oxygen pressure. The presented experimental data below were collected using two GCO films with 26 and 50 nm thicknesses.

The entire growth process was monitored by *in situ* high-pressure RHEED. The representative RHEED pattern of the 26-nm-thick GCO film is shown in Fig. 5(a). The intensity of the specular reflection shows only an initial reduction at the start of the deposition followed by intensity recovery. As the growth sequence progressed, it remains nearly constant without any evident oscillations. The elongated RHEED streaks with intensity modulation in Fig. 5(a) indicate the presence of a multilevel stepped surface [32]. This leads to the relatively high average surface roughness of 630(10) pm as determined from the XRR data presented in Fig. 5(b). The AFM scans confirmed the presence of a stepped surface with a roughness of separate terraces as low as $S_a \sim 100$–200 pm, which is similar to the quality of the MAO substrate surface.

Our data also indicate that the 2D growth mode of GCO gradually turns into the 3D island mode as the thickness of film increases. This is evident by the occurrence of spotty (3D-transmission-like) patterns on the RHEED images for a 50-nm-thick film [38]. This growth mode leads to the films with a rough surface that is consistent with the absence of oscillations in the XRR spectrum of this film.

Next, we discuss the results of our diffraction experiments. The 00l scan of the 50-nm-thick GCO film shown in Fig. 5(c) contains two reflections of the GCO film (blue) apart from the substrate reflections (red). These peaks can be indexed as the (004) and (008) reflections of GCO, confirming the (001) orientation and absence of secondary phases. To compare the out-of-plane lattice parameter of the GCO film with the bulk, we convert the lattice parameters of MAO from the face-centered unit cell to the equivalent body-centered one ($a_I = a_F/\sqrt{2}$). Since the bulk GCO lattice parameters are $a = 5.593$ Å and $c = 9.395$ Å [24], for the MAO substrate ($a_F = 8.08$ Å) it would result in 2.15% in-plane tensile strain, shortening the out-of-plane lattice constant. Indeed, our diffraction data for the 25- and 50-nm-thick films yield out-of-plane values of 9.31 and 9.37 Å, respectively, consistent with the expected value of tensile strain. Note, the difference in the lattice constant for 25- and 50-nm-thick films implies a different degree of strain relaxation, which is also evident from the asymmetric shape of the (004) GCO peak in the inset of Fig. 5(c).

To further validate that the film is indeed the targeted $GeCu_2O_4$ phase, we carried out reciprocal space mappings (RSMs) on the same 50-nm film. A schematic illustration for the reflections in the reciprocal space is plotted in Fig. 6, on which the allowed and forbidden reflections of both GCO and MAO are shown. Here, we note that since the out-of-plane lattice parameter of the film significantly differs from the substrate (9.37 Å vs 8.08 Å), the peak positions of the substrate and film diverge considerably in the reciprocal space. As a result, one can barely perform a usual RSM which includes both substrate and film reflections together. Instead, we measured two separate scans around the MAO (206) peak and the expected position of GCO (116) peak.

Indeed, as seen in Fig. 6 the film peak was found in the predicted position, which further demonstrates the stabilization of the desired GCO phase. Critically, the measured Q_x of

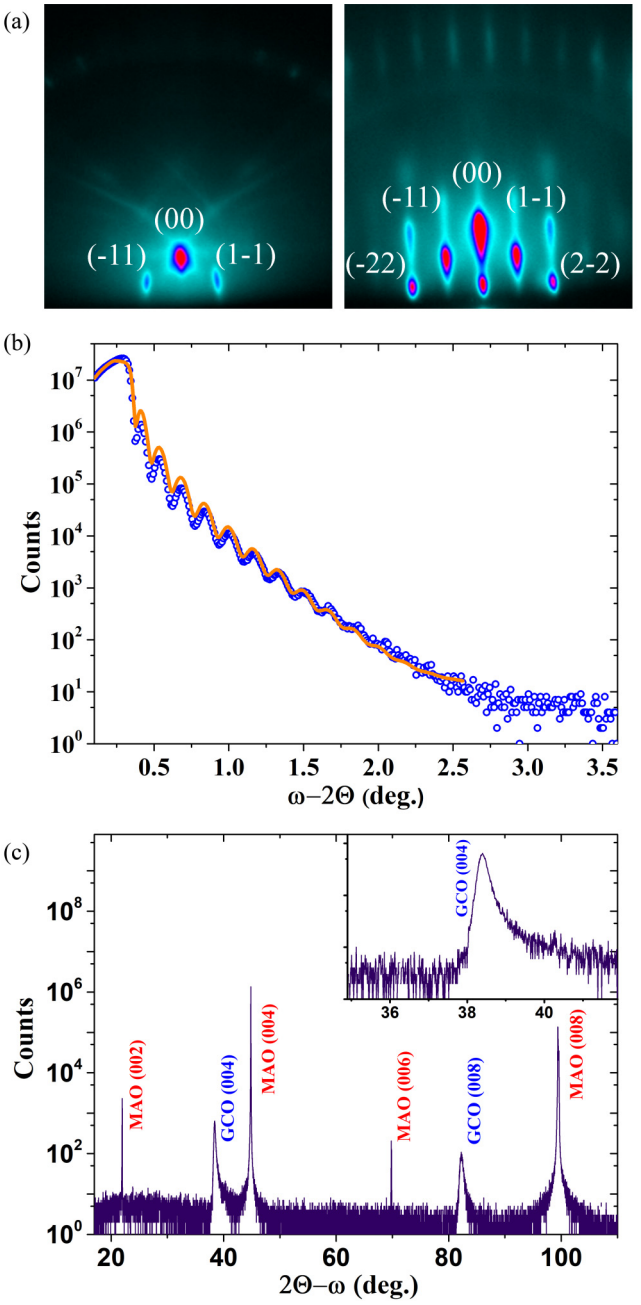

FIG. 5. Characterization of the grown GCO thin films. (a) The RHEED patterns of the MAO substrate and GCO film at 600 °C are on the left and right, respectively. (b) The fit of the XRR curve of this film yields a 26 nm film thickness. (c) 2Θ-ω x-ray diffraction scan along the 00l direction of another GCO film with 50 nm thickness. The scan contains allowed reflections of the substrate and fabricated film together with two forbidden reflections (002 and 006) of the substrate which arise because of the Umweganregung effect [31]. The inset shows asymmetric shape of the (004) GCO peak which indicates relaxation of the substrate-induced strain.

GCO (116) reflection is 0.1945(5) rlu, corresponding to the in-plane lattice parameter of 5.62 Å. This value is larger than 5.59 Å of bulk GCO, but smaller than 5.71 Å of the MAO substrate. Therefore, it implies an expected partial relaxation of strain inside the 50-nm film.

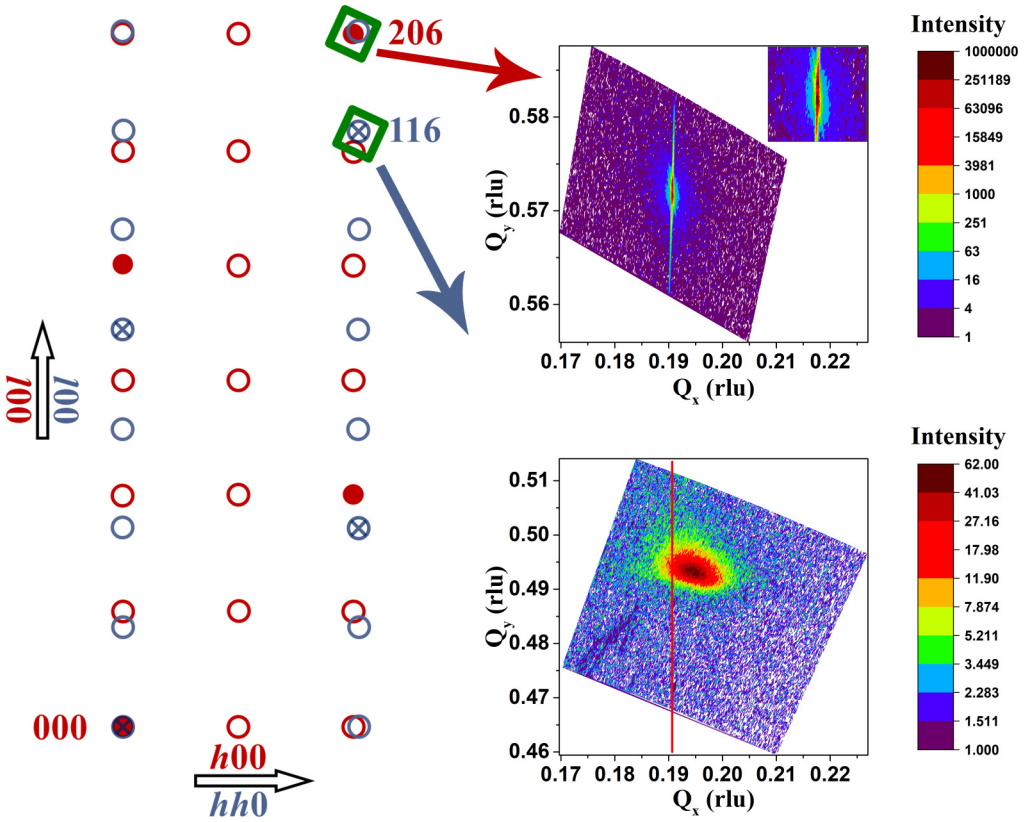

FIG. 6. Reciprocal space mapping of the 50-nm-thick GCO film. On the left the reciprocal lattices of the MAO substrate together with the GCO film are drawn for the case of (001) epitaxial growth. The solid and open red circles correspond to allowed and forbidden reflections of the MAO substrate, respectively, while blue circles designate reflections of the GCO film; in this case allowed reflections are marked by a crossed circle. The orientation of the scans coincides with the drawn reciprocal lattice, i.e., Q_x and Q_y are parallel to $h00$ and $00l$ directions of the substrate reciprocal lattice, respectively. The top-right figure is a scan around the 206 substrate reflection. The vertical stripe is due to nonmonochromaticity of the laboratory Cu $K\alpha$ source. The inset shows the zoomed 206 peak where one can see both $K\alpha_1$ and $K\alpha_2$ doublet peaks. The bottom-right figure is a scan around the 116 film reflection. The vertical red line designates the Q_x coordinate of the substrate peak.

We further verify the Cu oxidation state and the stoichiometry of the film by carrying out an XPS experiment on the 26-nm GCO film (see Fig. 7). The scan around the Cu $2p$ core state shows that a majority of copper ions have the expected 2+ oxidation state (935 eV $2p_{3/2}$ peak) with the well-developed satellite features shown in Fig. 7(b). However, a small feature seen at 933.5 eV (∼9% of total Cu signal) implies the presence of the Cu^{1+} state. This observation is consistent with the fact that our high-resolution scans around the $2p$ state of Ge and Cu yield Ge : Cu ≈ 1 : 1.2 which is also in variance with the bulklike $GeCu_2O_4$ composition. Since our XRD data do not show the presence

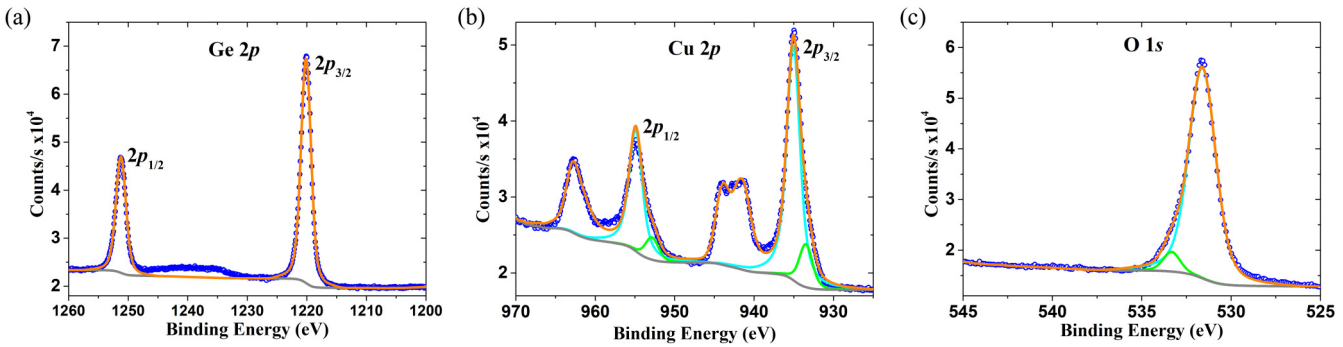

FIG. 7. High-resolution core-shell XPS scans of the 26-nm-thick GCO thin film: (a) Ge $2p$ shell, (b) Cu $2p$ shell, and (c) O $1s$ shell. The copper scan shows mostly Cu^{2+} (light-blue lines) with developed satellite features. The minor amount of Cu^{1+} and the different state of O (green lines) is likely related to the surface decomposition of the film.

of any additional peaks, in agreement with the absence of granulation in AFM scans common for multiphase films, we attribute the small admixture of Cu^{1+} and deviation in the cation ratio to the instability of the surface termination layer and/or degradation of the air-exposed surface of GCO films.

In summary, we have successfully fabricated single-crystalline epitaxial thin films of (001)-oriented $GeNi_2O_4$ with an $S = 1$ pyrochlore sublattice and the high-pressure phase of $GeCu_2O_4$ with a network of $S = 1/2$ linear chains. A combination of advanced spectroscopic and diffraction techniques confirmed the high structural and chemical quality of the films. The synthesis of coherently strained (001) $GeNi_2O_4$ thin films can provide additional opportunities for the study of unusual magnetic transitions in the $S = 1$ pyrochlore lattice and their response to the epitaxial strain. In addition, the availability of large-area $GeCu_2O_4$ thin films opens a road towards detailed experimentation to reveal the controversial nature of its ground state magnetism and elucidate the origin of multiferroicity in this compound.

Acknowledgments. The work in Rutgers University was supported by the Gordon and Betty Moore Foundation's EPiQS Initiative through Grant No. GBMF4534. This research used resources of the Advanced Light Source, a US DOE Office of Science User Facility under Contract No. DE-AC02-05CH11231.

[1] C. Lacroix, P. Mendels, and F. Mila, *Introduction to Frustrated Magnetism: Materials, Experiments, Theory*, Springer Series in Solid-State Sciences (Springer, Berlin, 2011).

[2] C. Castelnovo, R. Moessner, and S. Sondhi, Annu. Rev. Condens. Matter Phys. **3**, 35 (2012).

[3] L. Savary and L. Balents, Rep. Prog. Phys. **80**, 016502 (2016).

[4] Y. Zhou, K. Kanoda, and T.-K. Ng, Rev. Mod. Phys. **89**, 025003 (2017).

[5] C. Broholm, R. Cava, S. Kivelson, D. Nocera, M. Norman, and T. Senthil, Science **367**, eaay0668 (2020).

[6] H. Takagi and S. Niitaka, *Introduction to Frustrated Magnetism* (Springer, Berlin, 2011), pp. 155–175.

[7] M. K. Crawford, R. L. Harlow, P. L. Lee, Y. Zhang, J. Hormadaly, R. Flippen, Q. Huang, J. W. Lynn, R. Stevens, B. F. Woodfield, J. Boerio-Goates, and R. A. Fisher, Phys. Rev. B **68**, 220408(R) (2003).

[8] R. Stevens, B. F. Woodfield, J. Boerio-Goates, and M. K. Crawford, J. Chem. Thermodyn. **36**, 359 (2004).

[9] S. Diaz, S. de Brion, G. Chouteau, B. Canals, V. Simonet, and P. Strobel, Phys. Rev. B **74**, 092404 (2006).

[10] T. Lancaster, S. J. Blundell, D. Prabhakaran, P. J. Baker, W. Hayes, and F. L. Pratt, Phys. Rev. B **73**, 184436 (2006).

[11] M. Matsuda, J.-H. Chung, S. Park, T. Sato, K. Matsuno, H. A. Katori, H. Takagi, K. Kakurai, K. Kamazawa, Y. Tsunoda, I. Kagomiya, C. Henley, and S.-H. Lee, Europhys. Lett. **82**, 37006 (2008).

[12] J. C. Lashley, R. Stevens, M. K. Crawford, J. Boerio-Goates, B. F. Woodfield, Y. Qiu, J. W. Lynn, P. A. Goddard, and R. A. Fisher, Phys. Rev. B **78**, 104406 (2008).

[13] T. Yamada, Z. Hiroi, M. Takano, M. Nohara, and H. Takagi, J. Phys. Soc. Jpn. **69**, 1477 (2000).

[14] T. Zou, Y.-Q. Cai, C. R. dela Cruz, V. O. Garlea, S. D. Mahanti, J.-G. Cheng, and X. Ke, Phys. Rev. B **94**, 214406 (2016).

[15] L. Zhao, L. Muzica, U. Schwarz, and A. C. Komarek, Phys. Rev. Materials **2**, 041402(R) (2018).

[16] P. Yanda, S. Ghara, and A. Sundaresan, Solid State Commun. **272**, 53 (2018).

[17] K. Momma and F. Izumi, J. Appl. Crystallogr. **44**, 1272 (2011).

[18] K. Plumb, H. J. Changlani, A. Scheie, S. Zhang, J. Krizan, J. Rodriguez-Rivera, Y. Qiu, B. Winn, R. Cava, and C. L. Broholm, Nat. Phys. **15**, 54 (2019).

[19] E. Bertaut, V. Van Qui, R. Pauthenet, and A. Murasik, J. Phys. (Paris) **25**, 516 (1964).

[20] P. T. Barton, M. C. Kemei, M. W. Gaultois, S. L. Moffitt, L. E. Darago, R. Seshadri, M. R. Suchomel, and B. C. Melot, Phys. Rev. B **90**, 064105 (2014).

[21] T. Basu, T. Zou, Z. Dun, C. Q. Xu, C. R. Dela Cruz, T. Hong, H. B. Cao, K. M. Taddei, H. D. Zhou, and X. Ke, Phys. Rev. B **102**, 134421 (2020).

[22] S. Hara, Y. Yoshida, S.-I. Ikeda, N. Shirakawa, M. K. Crawford, K. Takase, Y. Takano, and K. Sekizawa, J. Phys. Soc. Jpn. **73**, 2959 (2004).

[23] J. Stewart, G. Ehlers, A. Wills, S. T. Bramwell, and J. Gardner, J. Phys.: Condens. Matter **16**, L321 (2004).

[24] W. Hegenbart, F. Rau, and K.-J. Range, Mater. Res. Bull. **16**, 413 (1981).

[25] M. Hase, I. Terasaki, and K. Uchinokura, Phys. Rev. Lett. **70**, 3651 (1993).

[26] M. Kohno, O. A. Starykh, and L. Balents, Nat. Phys. **3**, 790 (2007).

[27] O. A. Starykh, A. Furusaki, and L. Balents, Phys. Rev. B **72**, 094416 (2005).

[28] A. A. Tsirlin, R. Zinke, J. Richter, and H. Rosner, Phys. Rev. B **83**, 104415 (2011).

[29] D. I. Badrtdinov, V. V. Mazurenko, and A. A. Tsirlin, Phys. Rev. B **100**, 214401 (2019).

[30] O. Y. Gorbenko, S. Samoilenkov, I. Graboy, and A. Kaul, Chem. Mater. **14**, 4026 (2002).

[31] M. Renninger, Z. Phys. **106**, 141 (1937).

[32] S. Hasegawa, Reflection high-energy electron diffraction, *Characterization of Materials* (Wiley, Hoboken, NJ, 2012), pp. 1–14.

[33] K. Hirota, T. Inoue, N. Mochida, and A. Ohtsuka, J. Ceram. Soc. Jpn. **98**, 976 (1990).

[34] K. Persson, Materials Data on Ni_2GeO_4 (SG:227) by Materials Project, doi: 10.17188/1200493, The Materials Project, USA, 2016.

[35] Simulation was done using CRISPY software version 0.7.2 developed by M. Retegan. In the simulation we used a 0.9 reduction factor of default Slater integrals for Ni^{2+} in the software and the parameters $U_{3d,3d}$ and $U_{2p,3d}$ were 7.3 and 8.5 eV, respectively.

[36] M. W. Haverkort, M. Zwierzycki, and O. K. Andersen, Phys. Rev. B **85**, 165113 (2012).

[37] R. J. Hill, J. R. Craig, and G. Gibbs, Phys. Chem. Miner. **4**, 317 (1979).

[38] In this case the film thickness was determined from the number of laser pulses.